

# An RXTE Archival Search for Coherent X-ray Pulsations in LMXB 4U 1820–30

Rim Dib<sup>1</sup>, Scott M. Ransom<sup>1</sup>, Paul S. Ray<sup>2</sup>, Victoria M. Kaspi<sup>1</sup>, and Andrew M. Archibald<sup>3</sup>

## ABSTRACT

As part of a large-scale search for coherent pulsations from LMXBs in the *RXTE* archive, we have completed a detailed series of searches for coherent pulsations of 4U 1820–30 — an ultracompact LMXB with a binary period of 11.4 min, located in the globular cluster NGC 6624. The short binary period implies any coherent signal would be highly accelerated, so we used phase modulation searches, orbital-parameter-fitting coherent searches, and standard acceleration searches to give significant sensitivity to millisecond pulsations. We searched, in four energy bands and at a range of luminosities, a total of 34 archival *RXTE* observations, 32 of which had on-source integration times longer than 10 ks, and some of which were made consecutively which allowed us to combine them. We found no pulsations. Using our phase modulation search technique, which we ran on all 34 observations, we have been able to place the first stringent (95% confidence) pulsed fraction limits of  $\lesssim 0.8\%$  for all realistic spin frequencies (i.e.  $\lesssim 2$  kHz) and likely companion masses ( $0.02 M_{\odot} \leq M_c \leq 0.3 M_{\odot}$ ). Using our orbital-parameter-fitting coherent search, which we ran on only 11 selected observations, we have placed a pulsed fraction limit of  $\lesssim 0.3\%$  for spin frequencies  $\lesssim 1.25$  kHz and companion masses  $M_c \leq 0.106 M_{\odot}$ . By contrast, all five LMXBs known to emit coherent pulsations have intrinsic pulsed fractions in the range 3% to 7% when pulsations are observed. Hence, our searches rule out pulsations with significantly lower pulsed fractions than those already observed.

*Subject headings:* binaries: close — pulsars: general — stars: neutron — X-rays: binaries — X-rays: individual(4U 1820–30)

## 1. Introduction

One of the great scientific expectations when the Rossi X-ray Timing Explorer (*RXTE*) was launched in 1995 was the discovery of coherent pulsations from low-mass X-ray binaries (LMXBs). At present, only five accreting millisecond pulsars in LMXBs are known. All five are faint transient sources for which the pulsations at the spin period of the pulsar were discovered during outbursts (Wijnands & van der Klis

1998; Markwardt et al. 2002; Galloway et al. 2002; Markwardt, Smith, & Swank 2003a; Markwardt & Swank 2003).

Surprisingly, no pulsations have ever been seen in the non-transient X-ray emission from any LMXB. One possibility is that MSP coherent pulsations are smeared out by rapidly changing orbital Doppler shifts in short period binaries. Modern accelerated signal search techniques have not been applied systematically to many LMXBs so it is possible that there are millisecond pulsations in them that have gone unnoticed.

There are many things that we can learn from searching for more examples of direct pulsations from LMXBs. Coherent pulsations give the precise rotation rate of the neutron star and test the connection between recycled MSPs and LMXBs.

<sup>1</sup>Department of Physics, McGill University, Montreal, QC H3A 2T8

<sup>2</sup>E. O. Hulburt Center for Space Research, Code 7655, Naval Research Laboratory, Washington, DC 20375

<sup>3</sup>Department of Mathematics and Statistics, McGill University, Montreal, QC H3A 2K6

They help constrain the models of kHz QPOs and burst oscillations. Timing of the coherent pulses would also allow measurements of the accretion torques, the orbital parameters, and potentially the companion masses. In addition, in combination with X-ray and optical spectra, pulse timing can give information about the compactness and the equation of state of the neutron star. Finally, setting stringent upper limits on coherent pulsations in several sources in a variety of spectral states will impose constraints on the possible mechanism for suppression of the predicted coherent pulsations mentioned above. For these reasons, we have started a large-scale archival *RXTE* search for coherent pulsations from LMXBs, the first target of which is the ultracompact globular cluster LMXB 4U 1820–30.

This paper is organized as follows. In Section 1.1, we describe the general properties of 4U 1820–30. In Section 2, we describe the observations as well as the procedure we used to search for coherent pulsations. In Section 3, we describe our search techniques and the methods used to investigate the obtained candidate pulsation frequencies. In Section 4, we describe our results and derive our upper limits on possible coherent pulsations. Finally, in Sections 5 and 6, we discuss the implications of our findings and summarize.

### 1.1. Characteristics of 4U 1820–30

The source 4U 1820–30 is an atoll LMXB in globular cluster NGC 6624 (Stella, Priedhorsky, & White 1987). It has an orbital binary period of 685 s (11.4 min). The orbital period was identified to be the period of a nearly sinusoidal X-ray luminosity modulation with an amplitude of 2% to 3% and no strong energy dependence (Stella et al. 1987; Smale et al. 1987; Sansom et al. 1989; Tan et al. 1991; van der Klis et al. 1993; van der Klis et al. 1993; Chou & Grindlay 2001). A 16% modulation at a period of  $687 \pm 2.4$  s was also seen in the UV band (Anderson et al. 1997). This is the shortest known binary orbital period in an LMXB. 4U 1820–30 undergoes a regular  $\sim 176$  day accretion cycle (Priedhorsky & Terrell 1984) switching between high and low luminosity states, which differ by a factor of  $\sim 3$  in their luminosity (Stella et al. 1987). This luminosity variation makes 4U 1820–30 an attractive target for our search because it allows us to sample a fairly

large range of accretion rates in case the pulsations become visible only in some. In the low luminosity state, regular Type I bursts are seen  $\pm 23$  days around the minimum luminosity (Chou & Grindlay 2001). It is notable that burst oscillations have not been observed from this source. In the low state, 4U 1820–30 has also shown an extremely energetic superburst (Strohmayer & Brown 2002). This bursting behaviour confirms that the observed luminosity variations actually correspond to changes in the local accretion rate at the surface, and not just a geometrical effect, since they affect the bursting properties of the source. 4U 1820–30 also exhibits a variety of spectral states as can be seen from Figure 1. Several low frequency QPOs (Stella, Priedhorsky, & White 1987; Dotani et al. 1989; Wijnands, van der Klis, & Rijkhorst 1999). as well as two peaks of kHz QPOs (Smale, Zhang, & White 1997; Zhang et al. 1998; Kaaret et al. 1999) have been observed from this source. The separation between the two peaks is  $275 \pm 8$  Hz (van der Klis 1999). If the secondary star in the system is a white dwarf, its mass is estimated to be 0.058 to 0.078  $M_{\odot}$  (Rappaport et al. 1987). If the secondary is a main sequence star, the upper limit on its mass is 0.3  $M_{\odot}$  (Arons & King 1993).

Of all known LMXBs, we searched 4U 1820–30 first for several reasons. First, many high-time-resolution, long data sets are available in the archives. Second, the presence of kHz QPOs in this source may indicate favorable conditions for detecting pulsations. Third, its extremely short orbital period allows the use of the phase modulation search technique. This technique is most sensitive and provides the biggest increase in sensitivity over previous methods when the observations are longer than two complete binary orbits (Ransom, Cordes, & Eikenberry 2003). The precisely known and short orbital period also makes 4U 1820–30 one of only two LMXBs that can be searched using our fully coherent orbital-parameter-fitting search technique on a reasonable time scale.

The source 4U 1820–30 has previously been searched for coherent pulsations at frequencies under 50 Hz by Wood et al. (1991) and by Vaughan et al. (1994). Their upper limit on the pulsed fraction for sinusoidal pulses was 0.6% (95% confidence level), and 1.1% (99% confidence level) re-

spectively. Our searches cover a much wider frequency range, including, for the first time, the kHz range. This is particularly important since likely spin frequencies are near 275 Hz or 550 Hz, based on the kHz QPOs (van der Klis 1999; Chakrabarty et al. 2003).

## 2. Observations and Preliminary Data Preparation

We searched 34 archival *RXTE* PCA observations collected between 1996 and 2002 (see Table 1). All the observations were available in event modes with time resolutions of  $\sim 125 \mu\text{s}$ . 32 of the observations had a total time on source  $> 10$  ks. The longest of these was 29 ks with a total time on source of 16 ks. Some of the observations were segments of longer ones which allowed us to concatenate and analyse them together. The longest of the concatenated observations was 77.5 ks with a total time on source of 46.5 ks.

For each observation, we downloaded the files of raw events (one file for each *RXTE* orbit). The duration of an *RXTE* orbit (including Earth occultation time) is  $\sim 5.7$  ks. We filtered the files by selecting only events where the source elevation was  $> 10^\circ$ , the pointing offset was  $< 0.02^\circ$ , and where a minimum number of operational PCUs were on (see Table 1). We then transformed the arrival times of the events to the solar system barycenter using the ‘FTOOL’<sup>1</sup> FAXBARY. The barycentering was necessary to remove the effects of the spacecraft and Earth motions. We then split the data into four energy bands: Soft (2-5 keV), Medium (5-10 keV), Hard (10-20 keV), and Wide (2-20 keV), in order to attempt to maximize the signal-to-noise ratio of the unknown pulsations. This processing used custom Python scripts to call the standard ‘FTOOLS’. At the end of the preliminary data preparation we obtained four lists of events (photon arrival times) for every *RXTE* orbit in every observation, each list corresponding to one of the four energy bands.

## 3. Data Analysis

After we prepared the *RXTE*-orbit-long lists of events, we concatenated them into observation-long lists of events, and also broke them into much

shorter lists of events. We then binned the events into time series of different time resolutions (see Table 2) and searched them for pulsations using three types of searches which we summarize in Sections 3.1.1, 3.2.1, and 3.3.1. In Sections 3.1.2, 3.2.2, and 3.3.2, we explain how we used the three searches to obtain candidate pulsation frequencies. Finally, in Sections 3.1.3, 3.2.3, and 3.3.3, we explain the methods we used to investigate the obtained lists of candidate pulsation frequencies. All the data sets were processed on the 52-node dual 1.4 GHz Athlon-based Beowulf cluster operated by the McGill University Pulsar Group.

### 3.1. Acceleration Searches

#### 3.1.1. The Search Technique

This is the method traditionally used to compensate for the effects of orbital motion (e.g., Johnston & Kulkarni 1991): a time series is stretched or compressed appropriately to account for a trial *constant* frequency derivative (i.e. *constant* acceleration), Fourier transformed, and then searched for pulsations. We used a Fourier-domain variant of this technique based on matched filtering techniques which includes Fourier interpolation and harmonic summing of 1, 2, 4, and 8 harmonics to improve the sensitivity to non-sinusoidal pulsations (Ransom, Eikenberry, & Middleditch 2002).

Acceleration searches work best for systems where the orbital period  $\simeq 10 \times$  the observation length. Acceleration searches are not optimal for systems like 4U 1820–30 where the orbital period is shorter than the observation duration: the acceleration is not constant over the length of our time series. However, we chose not to run searches on time series shorter than 600 s (see Table 2) because we required a large number of photons. So while we did not expect acceleration searches to find pulsations, we still used them because they are included in our standard search pipeline. Also, the segmented acceleration searches that we ran, even though they were not short enough for the acceleration to be constant, can still be useful if a strong pulsed signal appears for a short period of time perhaps because the ‘weather’ on the surface briefly cleared and the pulsations appeared.

<sup>1</sup><http://heasarc.gsfc.nasa.gov/ftools/>

### 3.1.2. Obtaining Candidate Pulsation Frequencies

To run acceleration searches, we first binned the lists of events which we obtained in the data preparation into time series of different lengths and time resolutions (see Table 2). We performed an FFT on each of the time series and fed the result into a local red noise reduction algorithm which divides the FFT into continuous intervals the size of which increases logarithmically with frequency. The power in every bin of every interval is divided by the mean power in that interval. This produces FFTs that have a reduced signature of red noise. We then ran the acceleration searches on the obtained FFTs, searching for a maximum constant acceleration of  $a_{\max} < 5.1 \times 10^{10} / (fT_{\text{obs}}^2) \text{ m/s}^2$ , where  $f$  is the frequency of the detected pulsations in Hz, and  $T_{\text{obs}}$  is the integration time in seconds. For a signal of period 3 ms and an integration time of 600 s, this acceleration is  $425 \text{ m/s}^2$ . This number was chosen because it corresponds to the maximum length of a trial Fourier response template used in the search that would fit in the cache memory of the available machines. The maximum possible line of sight acceleration of 4U 1820–30 is  $a_{\max}(x) = 25240.6 \times x \text{ m/s}^2$  where  $x$  is the projected semi-major axis of the binary in light-seconds. For a companion mass of  $0.05 M_{\odot}$  and an inclination angle of  $60^\circ$ ,  $x = 13.4 \text{ lt-ms}$ , and  $a_{\max} = 339 \text{ m/s}^2$ .

Using acceleration searches, we searched for signals with an equivalent Gaussian significance  $\sigma > 2$  (Groth 1975) and with frequencies between 0.0375 Hz and 2048 Hz. We estimated  $\sigma$  based on the probability distribution of sums of powers in a normalized power spectrum (Groth 1975; Ransom et al. 2002). In order to correctly determine the significance of a candidate, we also took into account the number of independent trials in the searches (Ransom et al. 2002). Sometimes we increased the lower limit on the searched frequency to 1/8 Hz in order to eliminate the large number of low-frequency candidate oscillations that the red noise reduction routine did not successfully eliminate.

### 3.1.3. Candidate Follow-up

When our acceleration searches detect a candidate oscillation, they return values for the fre-

quency of the signal  $f$ , the frequency derivative  $\dot{f}$ , and the significance of the detection  $\sigma$ . Using the returned values for  $f$  and  $\dot{f}$ , we folded all acceleration candidates with  $\sigma > 3$ . Our folding software had the ability to fine tune the search in the  $f$  and  $\dot{f}$  directions. We also folded all the candidates with  $\sigma > 2$  that appeared in 15 or more observations to within 0.1% of their frequency. 0.1% was chosen because the frequency modulation caused by the the orbit of 4U 1820–30 will not cause  $f$  to deviate by more than 0.1% (see Section 3.2.1). All the folded candidates showed noise-like profiles.

## 3.2. Phase Modulation Searches

### 3.2.1. The Search Technique

In order to analyze longer observations we used the new ‘phase-modulation’ or ‘sideband’ search technique described by Ransom et al. (2003) (see also Jouteux et al. 2002). This technique relies on the fact that if the observation time is longer than the orbital period ( $T_{\text{obs}} \gg P_{\text{orb}}$ ), the orbit phase-modulates the pulsar’s spin frequency, resulting in a family of evenly spaced sidebands in the frequency domain, centered around the intrinsic pulsar signal for circular orbits (see for example Figure 2). The width of the region occupied by the sidebands is  $4\pi f x (T_{\text{obs}}/P_{\text{orb}})$  Fourier bins, where  $f$  is the frequency of the signal and  $x$  is the projected semi-major axis. The constant spacing between the sidebands is  $T_{\text{obs}}/P_{\text{orb}}$  Fourier bins.

A phase modulation search is conducted by taking short FFTs of portions of the full power spectrum of an observation. The short FFTs cover overlapping portions of various lengths (to account for the unknown semi-major axis of the LMXB) over all the Fourier frequency range of the original power spectrum (to account for the unknown pulsation period). The secondary power spectra are then searched for harmonically related peaks indicating regularly spaced sidebands (to detect the orbital period of the LMXB). Our phase modulation search included Fourier interpolation and harmonic summing of up to 4 harmonics of the orbital periods. This particular harmonic summing accounts for non-circular orbits, but not for non-sinusoidal pulsations. A detection provides initial estimates of the LMXB spin period, the orbital period, and the projected radius of the orbit. For interesting candidate oscillations, these estimates

are then refined by generating a series of complex-valued template responses (i.e. matched filters for the Fourier domain response of an orbitally modulated signal) to correlate with the original Fourier amplitudes (Ransom et al. 2003).

### 3.2.2. Obtaining Candidate Pulsation Frequencies

To run the phase modulation searches, we first concatenated the orbit-long lists of events which we had obtained at the end of the preliminary data preparation into observation-long lists of events. We then binned both the the observation-long and the orbit-long lists into time series (see Table 2). We performed an FFT on each, and fed the results into the local red noise reduction routine. We ran the phase modulation searches on the original FFTs as well as on the red noise-reduced FFTs. The obtained lists of candidate oscillations were almost identical: most of the candidates were millisecond pulsations so the red noise reduction did not affect them.

In order for the phase modulation search to detect a phase modulated signal, the short FFTs described in Section 3.2.1 must overlap at least a part of the phase modulated signal. When running the phase modulation searches on the observation-long data sets, we used the range of short FFT lengths derived in Ransom et al. (2003) that was appropriate for a wide range of orbital parameters: from 64 to 131072 bins. As we explained in Section 3.2.1, the spread of the phase modulated signal in the Fourier domain is proportional to  $xf$  where  $x$  is the projected semi-major axis in light-seconds and  $f$  is the intrinsic frequency of the signal. Because the maximum  $x$  for 4U 1820–30 is small (for the upper-limit companion mass of  $0.3 M_{\odot}$  and an inclination angle of  $90^{\circ}$ ,  $x = 1.02$  lt-s), the sizes of the short FFTs that we used would allow us to detect signals up to our Nyquist frequency (2048 Hz). We used a smaller range of short FFT sizes when we ran the phase-modulation search on the orbit-long data sets (64 to 32768 bins), and therefore were most sensitive to signal frequencies  $\lesssim 1$  kHz for all possible values of the companion mass.

### 3.2.3. Candidate Follow-up

For every candidate oscillation it finds, our phase modulation search returns, along with other

information, a pulsation period, an orbital period, and  $\sigma$ . We know from simulation that when a phase modulation search detects a signal with pulsed fraction equal to or greater than our upper limit calculated in Section 4.1, the pulsation period of the signal appears many times in the list of candidates obtained for that data set due to overlapping numerous short FFTs. Depending on the strength of the signal, there can also be a jump in the significance (measured in  $\sigma$ ) between the candidate oscillation corresponding to the real signal and the candidate with the next smaller significance. When this happens, if the list of candidates is arranged in order of decreasing  $\sigma$ , the real signal appears at the beginning of the list as an outlier with a singularly large  $\sigma$ .

When examining the phase modulation search candidates, we first extracted the candidates whose orbital period was 685 s within uncertainties. Among the extracted candidates, we searched for oscillation periods that appeared several times in any given observation. There were none. Also among the extracted candidates, we searched for candidates whose pulsation period appeared in the candidate lists of more than 10 observations to within a fractional period of 0.1%. There were also none. The 0.1% was a generous percentage considering that the uncertainties in the candidate pulsation periods were much smaller. Finally, we searched for outliers within the candidate lists. We did not find any.

## 3.3. Orbital-Parameter-Fitting Coherent Searches

### 3.3.1. The Search Technique

In this search, the source’s motion is modelled as a circular orbit. This is because LMXB accreting systems are known to have nearly circular orbits (Zahn 1977). Hence, we ignored the small errors due to a non-zero eccentricity. Three parameters are required to specify a particular circular orbit model: the orbital period  $P_{\text{orb}}$ , the projected semi-major axis in light-seconds  $x \equiv a \sin(i)/c$  (where  $a$  is the real semi-major axis,  $i$  is the inclination of the orbit, and  $c$  is the speed of light), and the orbital phase at the start of an observation  $\phi = 2\pi(T_{\text{start}} - T_{\text{o}})/P_{\text{orb}}$  (where  $T_{\text{start}}$  is the start time of the observation, and  $T_{\text{o}}$  is the time of the last ascending node before  $T_{\text{start}}$ ). Once

a set of trial orbital parameters is specified, it is straightforward to remove the shifts that the orbit would introduce in the arrival time of every photon. If the set of trial orbital parameters matches the real orbital parameters of the source, the resulting time series will contain the signature of an isolated pulsar that can be found using a standard pulsation search with no acceleration.

For 4U 1820–30, the orbital period is accurately known, but the other two parameters,  $x$  and  $\phi$ , must be searched. In Arons & King (1993), a maximum likely value  $x_{\max}$  for  $x$  is estimated, but the orbital phase is completely unknown. The sensitivity of detection to errors in the orbital parameters increases with pulsation frequency (see Section 4.2), so one must also estimate the highest likely pulsation frequency  $f_{\max}$ . From the sensitivity calculations in Section 4.2 we know that the number of sets of trial orbital parameters increases as  $(x_{\max}f_{\max})^2$ . For 4U 1820–30, reasonable estimates of these numbers can be provided (see next Section), and the effort required to search the data is feasible.

### 3.3.2. Obtaining Candidate Pulsation Frequencies

The method used to run searches by orbital-parameter-fitting is essentially the same as the standard method for running acceleration searches: the arrival times of the photons were time-shifted (this time to account for a *variable* orbital acceleration), and the resulting data sets were searched for isolated pulsar signatures. In particular, no matched filtering in the Fourier domain was done. The current implementation requires about 2000 hr to search a typical 4U 1820–30 observation on our computers. This is why it was necessary to limit the number of observations on which to run the search.

Chou & Grindlay (2001) did a folded period searching of the combined 1996-1997 *RXTE* standard2 observations of 4U 1820–30. They obtained an orbital period of  $P_{\text{orb}} = 685.0144 \pm 0.0054$  s. They then did a phase analysis combining the *RXTE* 1996-1997 observations of 4U 1820–30 with pre-*XTE* data and found an orbital period of  $P_{\text{orb}} = 685.0119 \pm 0.0001$  s. The uncertainties in both figures are small enough (see Section 4.2) that we did not need to search over this parameter. The decay in  $P_{\text{orb}}$  due to emission of gravita-

tional radiation, estimated to be  $\sim 0.00018$  s yr $^{-1}$  (Wagoner 1975), fell within the above uncertainties. We used  $P_{\text{orb}} = 685.014$  s when we ran our orbital-parameter-fitting search on 4U 1820–30.

The maximum plausible  $x$ , assuming the companion is a degenerate star is 0.024 lt-s (this corresponds to a companion mass of  $0.078M_{\odot}$  for an edge-on inclination). With our orbital-parameter-fitting search, we searched up to an  $x_{\max}$  of 0.032 lt-s (corresponding to a companion mass of  $0.106M_{\odot}$  for an edge-on inclination). Larger companion masses are allowed for smaller inclinations). We also set an upper bound on searched pulsation frequency of  $f_{\max} = 1250$  Hz to save computer time. If a set of trial orbital parameters corresponds exactly to the real orbital parameters of 4U 1820–30, our orbital-parameter-fitting search collects successfully all the power due to the signal. If our trial orbital parameters are slightly off, there will be a sensitivity loss. When we ran the search, we tuned the parameter steps to accept up to 50% loss in signal power at the maximum frequency. (As frequency decreases or the error in the size of the orbit decreases, this loss decreases to very near zero; see Section 4.2).

Based on calculations by in Middleditch (2004), and using the above known properties of 4U 1820–30 and the above mentioned maximum loss in signal power, we calculated that the error in a trial  $x$  should be no more than 0.000143 lt-s (see Section 4.2 for details). With that in mind, we generated an optimal grid of trial orbital parameter sets. The grid contained several thousands of points (see Section 4.2)

For each set of trial orbital parameters, we ran a separate search. We time-shifted the event data, to reflect the trial orbital parameters. We then binned it at a resolution of 0.244 ms and computed its Fourier transform. We applied our local red-noise reduction code and fed the result to our standard acceleration search code with a maximum acceleration of zero and an increased significance threshold (i.e.  $\sigma > 3$ ); keeping in mind that the  $\sigma$  returned by the acceleration search after subtracting the time-shifts is an overestimate of the real  $\sigma$  of the signal. This is because the orbital-parameter-fitting coherent search fails to take into account the number of times accelerations searches were run. The resulting list of candidate oscillations was then stored and the process

was repeated for the next set of trial orbital parameters.

### 3.3.3. Candidate Follow-up

Each candidate returned by the orbital-parameter-fitting code included a pulsation frequency  $f$ , an orbital amplitude  $x$ , an orbital phase  $\phi$ , and a significance  $\sigma$ . Using the returned values for  $f$ ,  $x$ , and  $\phi$ , we folded all the candidates with  $\sigma > 5$ , allowing the folding program to search a small distance in the frequency space. Most of the folded candidates showed noise-like profiles. None of the candidates corresponding to the more promising-looking folds appeared in more than one observation except for one candidate. This candidate appeared in two observations. However, the fold of the second detection of this candidate showed a noise-like profile.

Since folding the statistically significant candidates did not return any interesting results, we looked for candidates that repeated in more than one observation (to within a fractional range of  $f_{\text{percent}} = 0.001\%$  and to within a difference in  $x$  of  $x_{\text{difference}} = (P_{\text{orb}} * f_{\text{percent}}) / (400\pi + 2\pi f_{\text{percent}})$  lt-s).  $f_{\text{percent}}$  and  $x_{\text{difference}}$  were derived taking into account the spacing between the trial values of  $x$  and the drop in the amplitude of the detected signal when the trial orbital parameters were slightly off. There were about 300 candidates that repeated in 2 observations, and 0 candidates that repeated in more than 2 observations. We grouped the 300 candidates into pairs. Assuming the orbital period of  $685.0119 \pm 0.0001$  s reported in Chou & Grindlay (2001), we checked if the orbits of the members of each pair were in phase with each other. In 18 of the pairs the two orbits were in phase. In all 18 cases the single trial significances of the members of the pairs were around  $3\sigma$ . Again, the folds of all 36 candidates showed noise-like profiles.

## 4. Results and Upper Limits

Our searches did not detect pulsations.

Since we ran the acceleration searches in a region where they are not optimized, they were much less sensitive than the other two searches that we used. Below we explain the procedure we used to set an upper limit on the pulsed fraction of pulsations from 4U 1820–30 detectable

with our phase modulation search technique and our orbital-parameter-fitting coherent search technique.

### 4.1. Phase Modulation Searches

The phase modulation searches that we ran on observation-long data sets were more sensitive than the searches that we ran on the orbit-long data sets (Ransom et al. 2003). In this section we present the procedure used to set an upper limit on the pulsed fraction using the more sensitive search.

First, to save computer time, we wrote a modified version of our search script that searched only a particular region of the FFT. We then ran this version of the search on several data sets containing simulated pulsations from 4U 1820–30 of various pulsed fractions, for a range of companion masses ( $0.02 M_{\odot} \leq M_c \leq 0.3 M_{\odot}$ ), and for several spin frequencies. For the purpose of the simulations, we assumed the known orbital period of 685 s, a typical *RXTE* observation duration (20.5 ks), a count rate of 2050 counts per second, an inclination angle of  $60^\circ$ , and a circular orbit. Figure 3 shows the results of the simulations for this type of search run on data sets containing fake 3 ms sinusoidal pulsations. Every point in the figure corresponds to 100 searched data sets. The shading of every point corresponds to the detected power of the signal. The power was then converted to probability and multiplied by the number of independent trials (roughly the original number of time bins) to convert it to  $\sigma$ . In Figure 3, the line of  $\sigma = 5$  indicates the value of our 95% confidence upper limit on the pulsed fraction for a signal period of 3 ms. This value varied between 0.55% and 1.0% (background unsubtracted) over the range of companion masses that we used. The value was unaffected by the background correction since the background was small compared to the source count rate: using the ‘FTOOL’ PCBACKEST, we estimated the background count to be 10 counts per second per PCU. This is only 2% of the typical count rate of the source. This means that if there were a 3-ms coherent pulsation coming from 4U 1820–30 with a pulsed fraction equal to or higher than the upper limit stated above, our searches would have detected it at  $\sigma \geq 5$  95% of the time. The upper limit on the pulsed fraction decreased slightly when the period of the signal was larger by a few milliseconds. This is because,

at longer spin periods, the width of the sidebands feature is smaller (see Section 3.2.1); and hence the power accumulated in each of the sidebands is greater. For example, for a 10-ms coherent pulsation, this value varied between 0.3% and 0.5% over the range of companion masses that we used. Similarly, the upper limit on the pulsed fraction increases for smaller spin frequencies.

Our upper limit on the pulsed fraction of possible signals from 4U 1820–30 is  $\sim 0.8\%$  for spin periods close to 3 ms. The pulsed fractions of the signals detected from the 5 LMXBs with known signal period ranged between 3% and 7%, for signal frequencies between 2 and 6 ms (Wijnands & van der Klis 1998; Markwardt et al. 2002; Galloway et al. 2002; Markwardt et al. 2003a; Campana et al. 2003).

#### 4.2. Orbital-Parameter-Fitting Coherent Searches

The goal of orbital-parameter-fitting is to achieve a sensitivity close to the sensitivity one would have if the pulsar were isolated. To achieve this, one must compute how densely to sample the three-dimensional space of orbital parameters. Such calculations have already been done by Middleditch (2004), but in this section we work through them with more details to better understand the effects of small errors in the trial orbital period.

First, assume that  $P_{\text{orb}}$  is known exactly. Then combine  $x$  and  $\phi$  into a single complex number  $X$

$$X = xe^{i\phi}.$$

If the pulsar emits sinusoidal pulsations at a frequency  $f$ , then the received signal will be

$$s(t) = \sin(2\pi f \left( t + \text{Re} \left( X_{\text{orb}} e^{2\pi i t / P_{\text{orb}}} \right) \right)),$$

up to a phase shift (which we will ignore). If the pulse profile is not sinusoidal, this transformation will happen equally to all harmonics; we will ignore this too.

Suppose that we remove the effects of the orbital motion by time-shifting the incoming events according to a model using the known  $P_{\text{orb}}$  but  $X = X_{\text{trial}}$ . The observed signal will then be

$$s(t) = \sin(2\pi f(t +$$

$$\begin{aligned} & \text{Re} \left( X_{\text{orb}} e^{2\pi i t / P_{\text{orb}}} \right) - \text{Re} \left( X_{\text{trial}} e^{2\pi i t / P_{\text{orb}}} \right) \\ &= \sin(2\pi f(t + \\ & \text{Re} \left( (X_{\text{orb}} - X_{\text{trial}}) e^{2\pi i t / P_{\text{orb}}} \right))). \end{aligned}$$

In other words, the effect will be exactly that of a residual phase modulation of complex amplitude  $X_{\text{orb}} - X_{\text{trial}}$ .

Such a phase modulation produces a comb-like pattern in the Fourier domain (see Figure 2). For narrow combs, the tallest peak is the central peak: the one at the true pulsation frequency. The amplitude of the central peak falls off as  $J_0(|X_{\text{orb}} - X_{\text{trial}}|2\pi f)$  where  $J_0$  is a 0<sup>th</sup> order Bessel function (Ransom et al. 2003; Middleditch 2004). Therefore, the sensitivity loss (in power) due to a residual phase modulation of size  $|X_{\text{orb}} - X_{\text{trial}}| = \varepsilon$  will be  $J_0(\varepsilon 2\pi f)^2$ . This means that if we search the  $X_{\text{orb}}$  space with a sufficient density to fall within  $\varepsilon$  of every plausible  $X_{\text{orb}}$ , we will detect the source with a sensitivity only a factor of  $J_0(\varepsilon 2\pi f)^2$  less than that we would have for an isolated pulsar. In other words, the residual time shifts need to be small compared to the pulsation period.

For this particular situation, we fixed the maximum  $|X|$  as 0.032 lt-ms,  $f_{\text{max}}$  as 1250 Hz, and the sensitivity factor as 0.5 at  $f_{\text{max}}$ . The maximum allowable residual  $X$  (which we called  $\varepsilon$ ) is then 0.000143 ms. With that in mind, we generated an optimal grid of trials for complex-valued  $X$ . It turns out that the optimal grid (the one where the parameter space is searched most efficiently) is a circle-packing array: a grid where the values of  $X_{\text{trial}}$  are distributed on the corners of equilateral triangles (e.g., Middleditch 2004). The point in the middle of every triangle is the point that is furthest away from the closest  $X_{\text{trial}}$  and therefore the distance between it and the closest  $X_{\text{trial}}$  should be  $\varepsilon = 0.000143$  lt-s. The spacing between any two guesses is then 0.000264 lt-s. The total number of trials of  $X$  is then the area of the complex  $X$ -plane containing the trials (roughly  $\pi x_{\text{max}}^2$ ) divided by the area covered by every  $X_{\text{trial}}$  (roughly  $\pi \varepsilon^2$ ). This amounts to an approximate number of 50000 trials per observation. With the trials of  $X$  distributed as we described, our worst case sensitivity to a given signal of frequency  $f$  is then  $J_0(0.000143 \times 2\pi f)^2 \times$  (the sensitivity to an isolated pulsar signal of frequency  $f$ ). At  $f = f_{\text{max}}$



the value of this factor is 0.5. Its value increases for signals of lower frequency. For  $f = f_{\max}/2$ , it is 0.85.

In the above calculation, we assumed no loss of power due to errors in the assumed orbital period. But how accurately *does*  $P_{\text{orb}}$  need to be known? We can do an approximate calculation: suppose that  $P_{\text{trial}} = (1 - \epsilon)P_{\text{orb}}$ . The resulting signal is then

$$\begin{aligned} s(t) &= \sin(2\pi f(t + \\ &\quad \text{Re}\left(X_{\text{orb}}e^{2\pi it/P_{\text{orb}}}\right) - \text{Re}\left(X_{\text{trial}}e^{2\pi it/P_{\text{trial}}}\right))) \\ &\simeq \sin(2\pi f(t + \\ &\quad \text{Re}\left((X_{\text{orb}} - X_{\text{trial}}e^{2\pi i t \epsilon/P_{\text{orb}}})e^{2\pi it/P_{\text{orb}}}\right))). \end{aligned}$$

This amounts to an additional slowly-varying error in the estimation of the orbital phase  $\phi$ . Errors in  $\phi$  that are independent of  $(P_{\text{orb}} - P_{\text{trial}})$  have already been taken into account by the earlier sensitivity calculations. Therefore, when we calculated the effects of the additional slowly-varying error in  $\phi$  in a given observation of length  $T_{\text{obs}}$ , we could assume, to start with, that  $\phi$  is correct in the middle of that observation. At the end of that observation, we would have accumulated an error of size  $\epsilon\pi T_{\text{obs}}/P_{\text{orb}}$  in the estimation of  $\phi$ . This adds an *additional* residual  $X$  of about  $\epsilon|X|\pi T_{\text{obs}}/P_{\text{orb}}$ . In the worst case, this is about  $4.3\epsilon$  lt-s. From the difference between the value we used for the orbital period (685.014 s) and the lower bound on the more accurate orbital period measured in Chou & Grindlay (2001) of  $685.0119 \pm 0.0001$  s, we estimate  $\epsilon \sim 0.000003$ . Hence the size of the maximum additional residual  $X$  is  $\sim 0.000013$  lt-s, which is a factor of  $\sim 11$  smaller than the maximum residual  $X$  that the spacing in our grid of trials is allowing. In the worst case scenario (at  $f = f_{\max}$  and  $x = x_{\max}$ ), if we combine the maximum error in  $X$  due to the spacing of our trials with the additional error in  $X$  due to the error in the orbital period, we find a worst case sensitivity of  $0.43 \times$  that for an isolated pulsar (instead of 0.5 when the  $P_{\text{orb}}$  is exactly right). If the error caused by the uncertainty in  $P_{\text{orb}}$  were slightly larger, it would have caused an even larger decrease in the detectable power, and we would have been forced to search in  $P_{\text{orb}}$  also.

Above, we have extracted formulae for the sensitivity of the orbital-parameter-fitting search in

terms of the sensitivity of searches for an isolated pulsar. These, as well as a small number of simulations, show the following: if there are no errors in the search parameters, we can detect at  $3\sigma$  a signal of pulsed fraction 0.17%, and at  $5.3\sigma$  a signal of pulsed fraction 0.2%. If our trials for the orbital parameters (including the orbital period) are off by the worst-case amounts, we can detect at  $3\sigma$  a signal of pulsed fraction 0.26%, and at  $5.3\sigma$  a signal of pulsed fraction 0.3%. The above numbers are summarized in Table 3. Because of the way we are doing the candidate follow-up (i.e. folding candidates that appear several times in the list of candidates), the occurrence of the signal in more than one observation increases greatly the chance of detecting it: if a signal appeared only in one observation at  $3\sigma$ , we would have discarded it as a false candidate. If a signal appeared in several observations at  $3\sigma$  we would certainly not have missed it. Finally, any individual signal that appeared at  $\sigma \geq 5.3$  would have been detected with confidence.

To summarize, our sensitivity formulae and our simulations show reliable detection at a pulse fraction of 0.3% for the parameters we have chosen. This is of course dependent on a number of assumptions: the companion must be a degenerate star, the pulsation frequency must be less than about 1250 Hz, and  $P_{\text{orb}}$  must be within 0.0022 ms of 685.014 ms. It should be noted, however, that these assumptions are covariant: if the pulsation frequency is lower, the sensitivity improves. If  $x$  is smaller than the assumed upper bound, we become less sensitive to an error in  $P_{\text{trial}}$ .

## 5. Discussion

The search described in this paper represents the first source in a larger program to search for coherent pulsations in the persistent LMXBs. There are currently five known accreting MSPs, all of which have pulse frequencies in the range of 185 to 435 Hz and low luminosities. The pulsed fractions observed are in the 3 – 7 % range. Recently, observations of burst oscillations, kHz QPOs, and coherent pulsations in two of these accreting MSPs have confirmed that the burst oscillations are indeed at the spin frequency (Chakrabarty et al. 2003; Markwardt, Strohmayer, & Swank 2003b) and that the kHz QPO separation can be ei-

ther near the spin frequency or half the spin frequency. Thus, there is now a total sample of 14 LMXBs with well-determined spin frequencies. In 5 LMXBs, coherent pulsations are observed (Wijnands & van der Klis 1998; Markwardt et al. 2002; Galloway et al. 2002; Markwardt et al. 2003a; Markwardt & Swank 2003). In 11 LMXBs burst oscillations are observed (Strohmayer 2001; Strohmayer et al. 2003). In 2 of these LMXBs, both coherent pulsations and burst oscillations are observed (Chakrabarty et al. 2003; Strohmayer et al. 2003).

We can see pulsations during X-ray bursts and in the non-burst emission in a handful of transient sources. Why then can we not see pulsations in the persistent emission of the many bright LMXBs including 4U 1820–30?

For any individual pulsar, an unfavorable viewing geometry or rotational geometry can prevent the pulsations from being seen. However, a systematic absence of pulsations from all persistent LMXBs would require a stronger explanation. There are three main categories of explanations that have been considered. These are: relativistic effects that decrease the observed pulsed fraction, smearing of pulses from the surface due to electron scattering, and surface magnetic fields that are too weak to significantly channel the accretion flow (possibly as a result of magnetic screening). We briefly consider each of the possibilities below.

In Wood, Ftaclas, & Kearney (1988), the authors demonstrate that gravitational light-bending effects on emission from hot polar caps can greatly reduce the pulsed fraction: the pulses are distorted and the pulsed fraction decreases as a star becomes more relativistic because its radius is decreasing. The decrease in the pulsed fraction results from the fact that the gravitational deflection of photons displaces the horizon away from the observer. In other words, more of the star than a hemisphere is visible to the observer. Thus, one of the caps is always in nearly full view as the other is disappearing. It is possible for the pulsed fraction of a given source to be reduced down to  $\sim 1\%$ , provided the radius of the emitting star is small enough and the opening angle of the polar caps is large enough (Meszaros, Rifert, & Berthiaume 1988). This fraction is larger than our upper limit on the pulsed fraction, suggesting that gravitational lensing effects may not

be the only factor preventing us from seeing the pulsations. Also, the five known accreting MSPs exhibit pulsed fractions of more than 5%. There is no reason to believe that those systems have a significantly different value of  $M/R$  than the persistent LMXBs. Consequently, it seems that the relativistic effects are not the primary explanation for the small pulsed fraction in the latter sources.

Another explanation for low modulation fractions, electron scattering, has been revisited by Titarchuk, Cui, & Wood (2002). The existence of a corona (a spherical cloud) of hot electrons surrounding the accreting star has been inferred from the analysis of the X-ray spectra of several LMXBs (e.g., Kylafis & Klimis 1987; Titarchuk et al. 2002). This hot corona is presumably up-scattering softer seed photons and smearing out the pulsations. Titarchuk et al. (2002) argue that it is because of the large optical depth of this corona that pulsations have not been detected from most LMXBs. They claim that the optical depth below which millisecond pulsations become detectable is  $\tau \sim 4$ . They also do spectral fits for several LMXBs and extract the parameter  $\tau$ . For the majority of the analysed LMXBs they find that the optical depth of the Compton cloud is at least twice as high as  $\tau = 4$ . For these LMXBs, they claim that any high frequency pulsations (higher than  $\sim 300$  Hz) would be below detectability. Titarchuk et al. also make the observation that there is a possibility of finding pulsations in the sources that are much less luminous, because in these sources, the spherical Compton cloud is more transparent ( $\tau < 4$ ). Unfortunately, the smallest reported  $\tau$  for the spherical Compton cloud that is presumably surrounding 4U 1820–30 was  $\tau = 6$  (Bloser et al. 2000). In all the other papers that discuss spectra from 4U 1820–30, the authors used a Comptonization model with a black body component to fit the spectra and found that  $\tau$  falls between 11 and 13 (e.g., White, Stella, & Parmar 1988). If what Titarchuk et al. (2002) have claimed is true, the large optical depth of the Comptonizing cloud could very well be the reason we are not seeing pulsations from 4U 1820–30.

The possibility of magnetic screening by accreted material at high accretion rates has been examined by Cumming, Zweibel, & Bildsten (2001). Their reasoning goes as follows: to get preferential heating of the stellar surface, the mag-

netic field must be large enough to disrupt the accretion flow and channel it onto the polar caps. Preferential heating of the surface causes the observed emission to be pulsed. If the accretion flow is not disrupted by a magnetosphere, the accretion disk is believed to extend almost to the stellar surface and pulsations are no longer seen. This could happen because the external dipole magnetic field of the star is ‘buried’ or ‘screened’ by the accreted matter. Cumming et al. (2001) study the ‘burial’ scenario. In particular, they study the competition between downward compression of the magnetic flux by accretion at a given  $\dot{M}$ , and its upward transport by diffusion. They find that the diffusion and accretion time scales are equal for  $\dot{M} \sim 0.1\dot{M}_{\text{Edd}}$ , where  $\dot{M}_{\text{Edd}}$  is the accretion rate given by the Eddington limit. This means that for larger  $\dot{M}$  there is little chance that magnetic flux makes it to the surface and therefore little chance of observing pulsations. They also find that magnetic screening is completely ineffective for  $\dot{M} < 0.02\dot{M}_{\text{Edd}}$ , so that, no matter how the accreted material joins onto the star, the underlying stellar field would always be evident. The typical range of mass accretion rates in LMXBs is  $\dot{M} \geq 0.01\dot{M}_{\text{Edd}}$  ( $\dot{M} \geq 10^{-10} \text{ M}_{\odot} \text{ yr}^{-1}$ ) (Chakrabarty et al. 2003). Cumming et al. (2001) propose that the absence of persistent millisecond pulsations from most neutron stars in LMXBs is due to their high accretion rates. Discoveries made since then are consistent with their hypothesis: all five persistent millisecond X-ray pulsars are low-luminosity transients in very close binaries that lie at the low end of the mean  $\dot{M}$  distribution for LMXBs with  $\dot{M} \sim 10^{-11} \text{ M}_{\odot} \text{ yr}^{-1}$  (Galloway et al. 2002; Campana et al. 2003; Chakrabarty et al. 2003). It is tempting to adopt magnetic screening as the main explanation for the lack of observed pulsations from 4U 1820–30 because the luminosity of this source ( $\sim 4 \times 10^{37} \text{ ergs/s}$ ) is on the high end of luminosities of atoll sources, implying a normal (rather than a low) accretion rate of the in-falling matter. Stella et al. (1987) estimated this accretion rate to be  $\sim 5 \times 10^{-9} \text{ M}_{\odot} \text{ yr}^{-1}$ .

## 6. Summary

In this paper, we have described a search of 4U1820–30 that set upper limits on the pulsed fraction covering essentially all plausible pulse periods and companion masses for this system.

These limits were between 0.3% and 0.8% over this whole range. We also searched a broad range of luminosity and spectral states (see Figure 1). The luminosities covered the range from 0.08 to 0.25 of the Eddington luminosity for a  $1.4 \text{ M}_{\odot}$  neutron star and a distance of 6.4 kpc. 4U1820–30 is interesting in this regard because the luminosity varies by a factor of three.

For 4U 1820–30, our upper limits are about an order of magnitude lower in pulsed fraction than the known accreting MSPs. However, this is only one source and any number of specific features, such as unfavorable viewing or rotational geometries, in addition to electron scattering and magnetic screening, could prevent the pulsations from being seen. The most interesting conclusions will be drawn once we have a sample of many more sources that have been searched to similarly deep levels.

This work was supported by the Natural Sciences and Engineering Research Council (NSERC) Julie Payette research scholarship. It would also have been impossible to do this work without the computing power of the Beowulf computer cluster operated by the McGill University Pulsar Group and funded by the Canada Foundation for Innovation. Additional support came from NSERC, FQRST, CIAR, and NASA. Victoria M. Kaspi is a CRC Chair and NSERC Steacie Fellow.

## REFERENCES

- Anderson, S. F., Margon, B., Deutsch, E. W., Downes, R. A., & Allen, R. G. 1997, *ApJ*, 482, L69+
- Arons, J. & King, I. R. 1993, *ApJ*, 413, L121
- Bloser, P. F., Grindlay, J. E., Kaaret, P., Zhang, W., Smale, A. P., & Barret, D. 2000, *ApJ*, 542, 1000
- Campana, S., Ravasio, M., Israel, G. L., Mangano, V., & Belloni, T. 2003, *ApJ*, in preparation.
- Chakrabarty, D., Morgan, E. H., Munro, M. P., Galloway, D. K., Wijnands, R., van der Klis, M., & Markwardt, C. B. 2003, *Nature*, 424, 42
- Chou, Y. & Grindlay, J. E. 2001, *ApJ*, 563, 934

- Cumming, A., Zweibel, E., & Bildsten, L. 2001, *ApJ*, 557, 958
- Dotani, T., Mitsuda, K., Makishima, K., & Jones, M. H. 1989, *PASJ*, 41, 577
- Galloway, D. K., Chakrabarty, D., Morgan, E. H., & Remillard, R. A. 2002, *ApJ*, 576, L137
- Groth, E. J. 1975, *ApJS*, 29, 285
- Johnston, H. M. & Kulkarni, S. R. 1991, *ApJ*, 368, 504
- Jouteux, S., Ramachandran, R., Stappers, B. W., Jonker, P. G., & van der Klis, M. 2002, *A&A*, 384, 532
- Kaaret, P., Piraino, S., Bloser, P. F., Ford, E. C., Grindlay, J. E., Santangelo, A., Smale, A. P., & Zhang, W. 1999, *ApJ*, 520, L37
- Kylafis, N. D. & Klimis, G. S. 1987, *ApJ*, 323, 678
- Markwardt, C. B., Smith, E., & Swank, J. H. 2003a, *IAU Circ.*, 8080, 2
- Markwardt, C. B., Strohmayer, T. E., & Swank, J. H. 2003b, *The Astronomer's Telegram*, 164, 1
- Markwardt, C. B. & Swank, J. H. 2003, *IAU Circ.*, 8144, 1
- Markwardt, C. B., Swank, J. H., Strohmayer, T. E., Zand, J. J. M. i., & Marshall, F. E. 2002, *ApJ*, 575, L21
- Meszaros, P., Riffert, H., & Berthiaume, G. 1988, *ApJ*, 325, 204
- Middleditch, J. 2004, *ArXiv Astrophysics e-prints*
- Priedhorsky, W. & Terrell, J. 1984, *ApJ*, 284, L17
- Ransom, S. M., Cordes, J. M., & Eikenberry, S. S. 2003, *ApJ*, 589, 911
- Ransom, S. M., Eikenberry, S. S., & Middleditch, J. 2002, *AJ*, 124, 1788
- Rappaport, S., Ma, C. P., Joss, P. C., & Nelson, L. A. 1987, *ApJ*, 322, 842
- Sansom, A. E., Watson, M. G., Makishima, K., & Dotani, T. 1989, *PASJ*, 41, 591
- Smale, A. P., Mason, K. O., & Mukai, K. 1987, *MNRAS*, 225, 7P
- Smale, A. P., Zhang, W., & White, N. E. 1997, *ApJ*, 483, L119+
- Stella, L., Priedhorsky, W., & White, N. E. 1987, *ApJ*, 312, L17
- Stella, L., White, N. E., & Priedhorsky, W. 1987, *ApJ*, 315, L49
- Strohmayer, T. E. 2001, *Advances in Space Research*, 28, 511
- Strohmayer, T. E. & Brown, E. F. 2002, *ApJ*, 566, 1045
- Strohmayer, T. E., Markwardt, C. B., Swank, J. H., & in't Zand, J. 2003, *ApJ*, 596, L67
- Tan, J., Morgan, E., Lewin, W. H. G., Penninx, W., van der Klis, M., van Paradijs, J., Makishima, K., Inoue, H., Dotani, T., & Mitsuda, K. 1991, *ApJ*, 374, 291
- Titarchuk, L., Cui, W., & Wood, K. 2002, *ApJ*, 576, L49
- van der Klis, M. 1999, in *Pulsar Timing, General Relativity and the Internal Structure of Neutron Stars*, 259–+
- van der Klis, M., Hasinger, G., Dotani, T., Mitsuda, K., Verbunt, F., Murphy, B. W., van Paradijs, J., Belloni, T., Makishima, K., Morgan, E., & Lewin, W. H. G. 1993, *MNRAS*, 260, 686
- van der Klis, M., Hasinger, G., Verbunt, F., van Paradijs, J., Belloni, T., & Lewin, W. H. G. 1993, *A&A*, 279, L21
- Vaughan, B. A., van der Klis, M., Wood, K. S., Norris, J. P., Hertz, P., Michelson, P. F., van Paradijs, J., Lewin, W. H. G., Mitsuda, K., & Penninx, W. 1994, *ApJ*, 435, 362
- Wagoner, R. V. 1975, *ApJ*, 196, L63
- White, N. E., Stella, L., & Parmar, A. N. 1988, *ApJ*, 324, 363
- Wijnands, R. & van der Klis, M. 1998, *Nature*, 394, 344

Wijnands, R., van der Klis, M., & Rijkhorst, E.  
1999, ApJ, 512, L39

Wood, K. S., Ftaclas, C., & Kearney, M. 1988,  
ApJ, 324, L63

Wood, K. S., Hertz, P., Norris, J. P., Vaughan,  
B. A., Michelson, P. F., Mitsuda, K., Lewin,  
W. H. G., van Paradijs, J., Penninx, W., & van  
der Klis, M. 1991, ApJ, 379, 295

Zahn, J.-P. 1977, A&A, 57, 383

Zhang, W., Smale, A. P., Strohmayer, T. E., &  
Swank, J. H. 1998, ApJ, 500, L171+

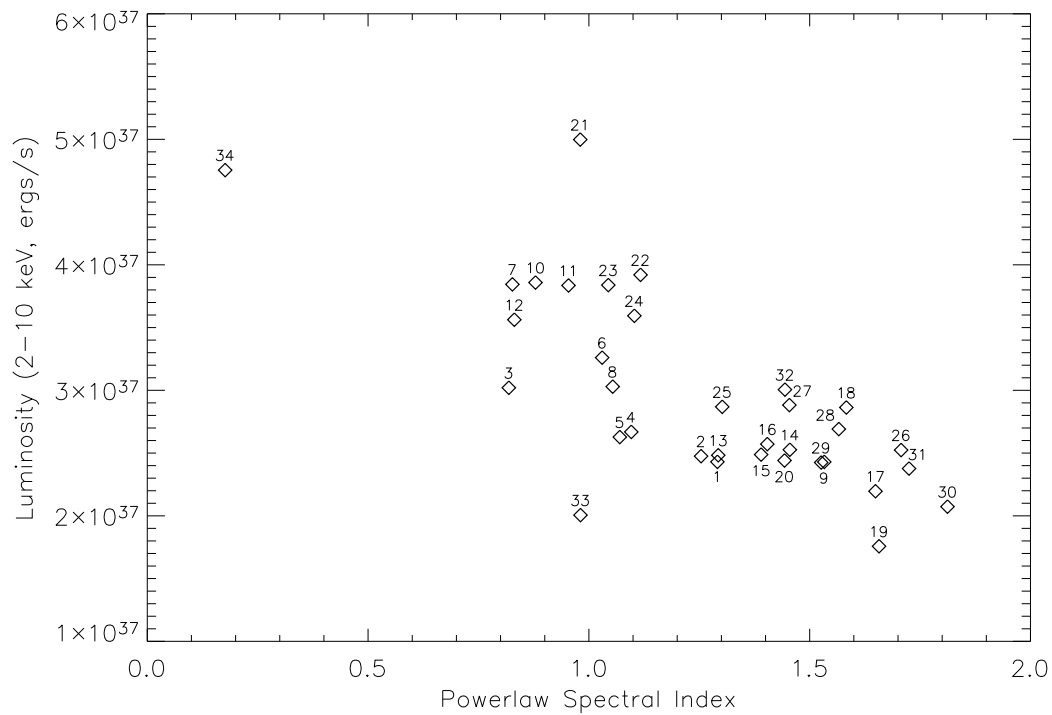


Fig. 1.— The power-law spectral index and the 2–10 keV luminosity of each of the 34 observations that we have searched for pulsations. These numbers were obtained from spectral fittings and were based on an assumed distance of 6.4 kpc.

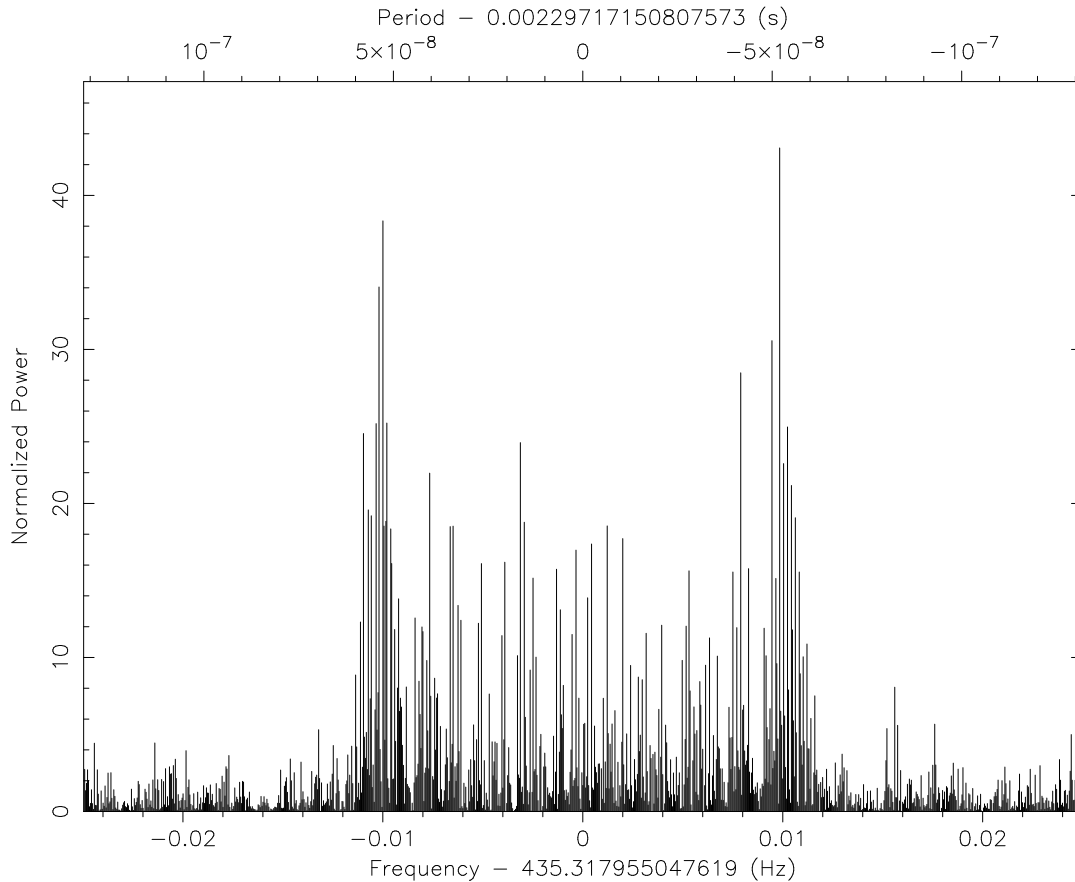


Fig. 2.— Sidebands in the FFT of observation 70131-01-05-00 (4 *RXTE* orbits long) of XTE J1751-305 centered on the intrinsic pulsar spin frequency (435.318 Hz) and caused by orbital phase modulations of the pulsar frequency (see Section 3.2.1). The binary orbital period that is causing the above modulation is  $\sim 42.4$  min and the projected orbital radius is  $\sim 10.11$  lt-ms. The pulsed fraction above is high (3.76%, background unsubtracted) which makes the signal stand well above the noise. The width of the sideband pattern is related to the projected semi-major axis of the orbit. The above signal was detected at  $10.6\sigma$  using our phase modulation search technique and at  $10.8\sigma$  using our acceleration search technique.

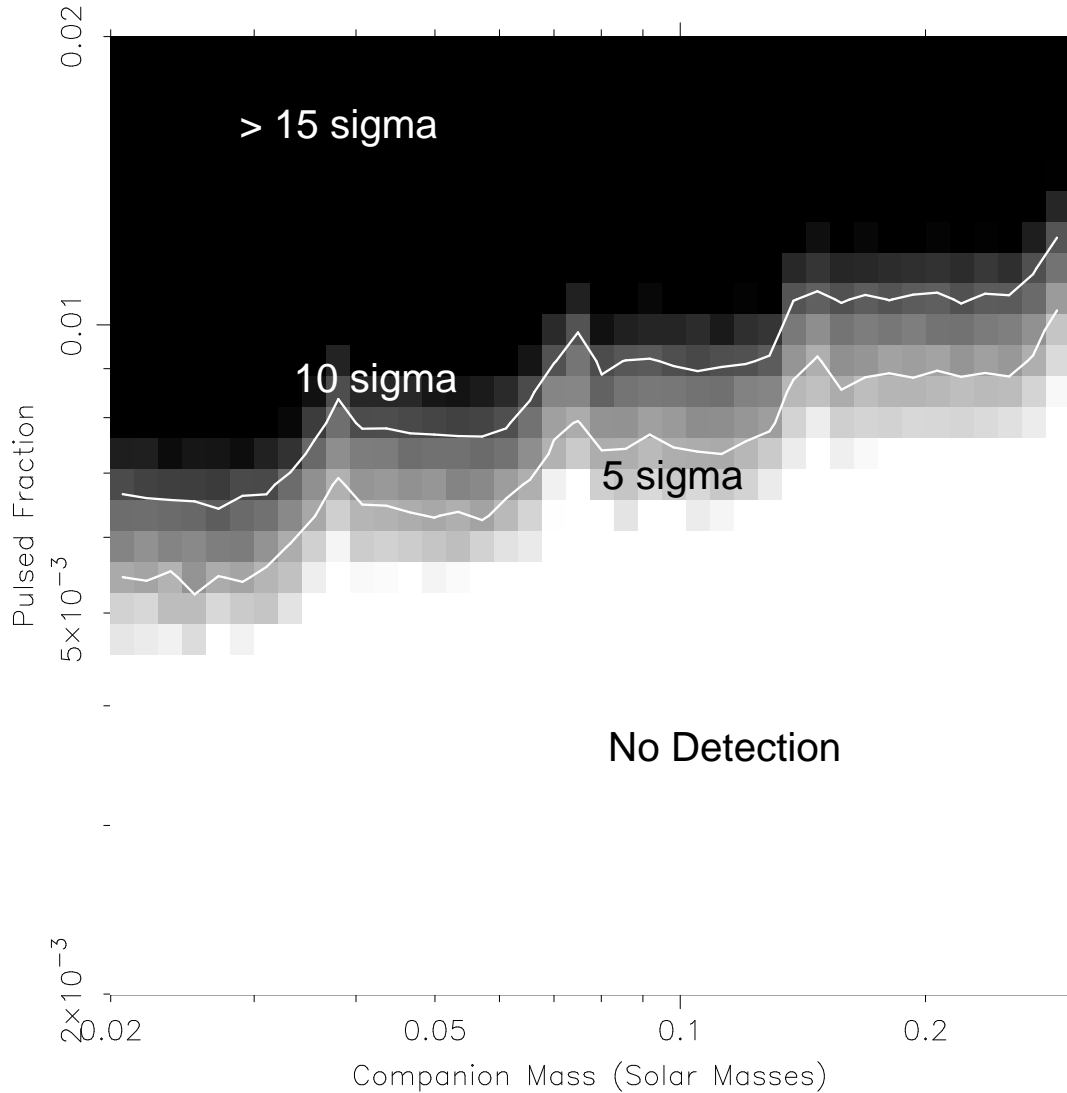


Fig. 3.— Monte-Carlo derived sensitivity calculations for the pulsation searches of archival *RXTE* observations of 4U 1820–30. The plotted sensitivities are 95% confidence limits using the phase modulation search technique for a typical *RXTE* observation assuming a pulsar spin period of 3 ms. With these types of searches, we would easily have detected any coherent pulsations with a pulsed fraction  $\gtrsim 0.8\%$  for all realistic companion masses and spin periods.



TABLE 1  
*RXTE* OBSERVATIONS<sup>a</sup> OF 4U 1820–30

	ObsID	Year	Start Time <sup>b</sup> (MJD)	Duration <sup>c</sup> (ks)	Time on Source (ks)	Count Rate <sup>d</sup> (counts/s/PCU)	Num PCUs <sup>e</sup>	Num Events <sup>f</sup> ( $\times 10^6$ )	Luminosity <sup>g</sup> ( $\times 10^{37}$ ergs/s)
1	10075-01-01-020	1996	50384.63103	28.0	18.2	450	5	38.56	2.4
2*	10075-01-01-02	1996	50384.96433	17.2	10.4	460	5	26.08	2.5
3	10075-01-01-030	1996	50386.49418	28.2	17.1	600 – 565	5	44.99	3.0
4*	10075-01-01-031	1996	50386.82749	25.2	16.4	565 – 455	4	42.17	2.7
5	10075-01-01-03	1996	50387.14749	3.1	3.1	480	4	7.50	2.6
6	20075-01-01-00	1997	50488.42272	24.9	16.0	635 – 550	5	48.30	3.3
7	20075-01-02-01	1997	50514.02219	17.9	11.1	725	5	42.19	3.8
8	20075-01-03-00	1997	50530.70491	20.0	13.1	585	3	33.96	3.0
9*	20075-01-04-00	1997	50548.70709	24.1	14.9	450	5	33.98	2.4
10*	20075-01-06-00	1997	50595.33191	15.3	11.3	720	5	41.23	3.9
11*	20075-01-08-00	1997	50645.22308	15.2	11.0	720	5	40.94	3.8
12*	20075-01-09-00	1997	50675.45754	25.1	16.0	670 – 735	4	51.31	3.6
13	30057-01-01-02	1998	50909.66291	18.4	11.2	470	4	24.24	2.5
14*	30053-03-01-000	1998	50920.19895	25.2	16.4	465	5	39.94	2.5
15	30053-03-01-001	1998	50920.52779	20.8	12.0	465	4	24.94	2.5
16*	30053-03-01-00	1998	50920.79458	25.8	13.2	475	5	41.05	2.6
17	30053-03-02-03	1998	51080.45284	20.9	14.2	430 – 380	4	22.30	2.2
18	40017-01-02-00	1999	51222.63887	20.9	14.4	510	4	33.63	2.9
19	40017-01-03-00	1999	51238.03748	15.1	10.4	320	5	16.81	1.8
20	40017-01-04-00	1999	51253.69624	18.9	10.5	430	4	13.42	2.4
21*	40017-01-07-00	1999	51300.07107	18.6	10.9	980 – 895	3	37.42	5.0
22	40017-01-09-00	1999	51330.51073	15.1	10.6	700	3	28.80	3.9
23	40017-01-12-00	1999	51389.38952	15.3	10.7	705	3	23.53	3.8
24*	40017-01-13-00	1999	51400.44912	21.0	14.7	660	3	28.88	3.6
25	40017-01-14-00	1999	51407.50805	15.1	10.6	505	5	27.13	2.9
26	30057-01-03-01	1999	51410.50430	24.0	15.1	515 – 445	3	24.59	2.5
27	30057-01-03-000	1999	51412.31866	29.0	16.9	495 – 530	3	34.10	2.9
28	30057-01-03-00	1999	51412.65197	7.5	5.1	510	4	10.74	2.7
29	40017-01-15-00	1999	51417.29843	20.4	12.8	440	3	17.05	2.4
30	40019-02-01-00	1999	51421.30667	25.0	15.3	370	3	16.81	2.0
31	30057-01-05-00	1999	51435.00244	26.8	17.9	365 – 480	2	26.34	2.4
32	40017-01-18-00	1999	51464.36730	20.8	14.0	535	3	26.07	3.0
33	40017-01-21-00	2001	51941.01232	14.9	10.4	380	4	14.36	2.0
34*	40017-01-23-01	2002	52355.88359	14.8	10.3	915	3	32.89	4.8

<sup>a</sup>We used event data with  $\sim 125 \mu\text{s}$  time resolution for all observations.

<sup>b</sup>Start time of the observation in MJD.

<sup>c</sup>Stop time – Start time of the observation in ks.

<sup>d</sup>Approximate photon count per second per PCU obtained from the Standard 2 lightcurve in the wide band (2–20 keV).

<sup>e</sup>Minimum number of PCUs in use at a given moment of the observation.

<sup>f</sup>Approximate total number of events processed in the wide band (2–20 keV).

<sup>g</sup>2–10 keV luminosities obtained from spectral fitting and based on an assumed distance of 6.4 kpc.

\*Observations marked with a \* were searched with acceleration searches, phase modulation searches, and an orbital-parameter-fitting coherent search. The remaining observations were searched only with acceleration searches and phase modulation searches.

TABLE 2  
SEARCH TYPES FOR DIFFERENT DATA FILE TYPES

Type of Data File	Searches Run
Observation-long lists of events	orbital-parameter-fitting coherent search <sup>a</sup> (W band only)
Observation-long time series binned at 0.244 ms	Acceleration searches (all bands), phase modulation searches (all bands)
<i>RXTE</i> -orbit-long lists of events	No searches run
<i>RXTE</i> -orbit-long time series binned at 0.122 ms	Acceleration searches (all bands), phase modulation searches (all bands)
600-s-long and 1500-s-long lists of events	No searches run
600-s-long and 1500-s-long time series binned at 0.122 ms	Acceleration searches (all bands) <sup>b</sup>

<sup>a</sup>Because running an orbital-parameter-fitting coherent search was extremely demanding computationally, we ran this search on event lists of 11 observations only. By contrast, we ran accelerations searches and phase modulation searches on time series of all 34 observations.

<sup>b</sup>The segmented acceleration searches that we ran, even though they were not short enough for the acceleration to be constant, could still be useful if a strong pulsed signal were to appear for a short period of time.

TABLE 3  
 RESULTS OF SENSITIVITY CALCULATIONS FOR THE  
 ORBITAL-PARAMETER-FITTING COHERENT SEARCHES

Pulsed Fraction	Best Case Detection $\sigma^*$	Worst Case Detection $\sigma^*$
0.17%	3	< 3
0.2%	5.3	< 3
0.26%	> 5.3	3
0.3%	> 5.3	5.3

\* $\sigma$  is an equivalent Gaussian significance.